THE TAGISH LAKE METEORITE FALL : INTERPRETATION OF FIREBALL PHYSICAL CHARACTERISTICS

P.Brown[1], D.O. ReVelle[1], and A.R. Hildebrand[2]

[1]Los Alamos National Laboratory, MS J577, Los Alamos, NM 87545 USA email:pbrown@lanl.gov
[2]Department of Geology and Geophysics, University of Calgary, Calgary, Alberta, CANADA

ABSTRACT

We have analyzed available instrumental and eyewitness records associated with the fireball leading to the fall of the Tagish Lake meteorite. Initial chemical and physical studies of this carbonaceous chondrite have shown it to be unique. It is one of the most primitive meteorites yet recovered and is physically weak. By determining the meteoroid trajectory, velocity, and physical breakup in the atmosphere, we can characterise the fireball as intermediate between Type II and Type IIIa, following the classification of Ceplecha et al. (1998). Modelling suggests an initial porosity for the pre-atmospheric meteoroid in the range 40-60%. The initial fragmentation occurred under less than 0.3 MPa dynamic pressure. Determination of Tagish Lake's orbit suggests a linkage to parent bodies in the main asteroid belt, though association with Encke-type comets cannot be strictly excluded. Tagish Lake may represent an intermediate object between chondritic asteroids and cometary bodies consistent with a linkage to D-class asteroids based on results from reflectance-spectra work.

1. INTRODUCTION

The Tagish Lake meteorite fell on January 18, 2000 at 16:43:43 UT (08:43:43 local time). The fireball accompanying the meteorite fall was widely observed over the Yukon Territory, British Columbia, portions of Alaska and the Northwest Territories . The fireball was of unusually long duration; many observers reported it to be visible for 15-20 seconds. That the duration of the event was significant is verified by a security video camera record which shows increased illumination of the local terrain from the fireball for just over ten seconds. The peak brightness of the fireball was enough to illuminate the still dark terrain to near daylight conditions for observers near the endpoint. The final portion of the fireball trajectory was dominated by one short burst followed by a more extended terminal disintegration. Reports from eyewitnesses invariably described these two major detonations as primary features of the event. Substantial delayed sounds were heard by observers at distances of up to 200 km from the fireball trajectory. In addition to these delayed sounds, several observations of electrophonic sounds (cf. Keay et al., 1980) were also reported. Particularly notable are several reports of unusual smells being detected at nearly the same time, to slightly following, the passage of the fireball proper. Observers uniformly reported these smells to be of a foul metallic, chemical or sulfurous odour.

In addition to these eyewitness records, a total of five video records and 24 still photographs of the associated dust cloud were provided by witnesses. Figure 1 shows an example of the still photos taken shortly after the fireball. In addition to these data, sensors on US Department of Defence satellites detected the event in the infrared (providing positional information) and at optical wavelengths (defining the light curve). The space-based recordings include a fortuituous image of the dust-cloud made by the Defence Meteorological Satellite Program F-13 satellite which scanned the area including the endpoint of the fireball only two minutes after the event. Figure 2 shows this image of the associated dust cloud.

The airwave signal from the fireball was recorded on three local seismic stations, Whitehorse (WHY), Haines Junction (HYT) and Dease Lake (DLBC). These show both direct air-coupled Rayleigh wave arrivals, the airwave itself as well as seismically coupled body waves due to the airblast.

Of great value in constraining interpretation of the fireball data is the recovery of meteorites from the ice surface of the Taku Arm of Tagish Lake over the interval January - May, 2000 (cf. Brown et al., 2000). In total some 410 individual fragments from the fireball were located and more than 200 samples recovered for later analysis, totalling approximately 5 kg of material. Based on the available fall data, the physical characteristics of the recovered samples, and modelling of the event, here we attempt to reconstruct the pre-atmospheric orbit and physical character of the Tagish Lake meteoroid.

Figure 1. Dust cloud remaining after the passage of the Tagish lake fireball. This image was still-framed captured from video of the dust cloud shot by Doug Davidge from Whitehorse, Yukon Territory several minutes after the fireball. The recording was made using a Sony TRV75 Hi-8 camcorder equipped with extended infrared response. The bright portion of the trail near the lower part of the image represents that segment of the trail where the sun is within a few degrees of rising above the local horizon. This fact coupled with the enhanced dust deposition near the end of the trail is the probable reason this portion appears so much brighter than the rest of the trail.

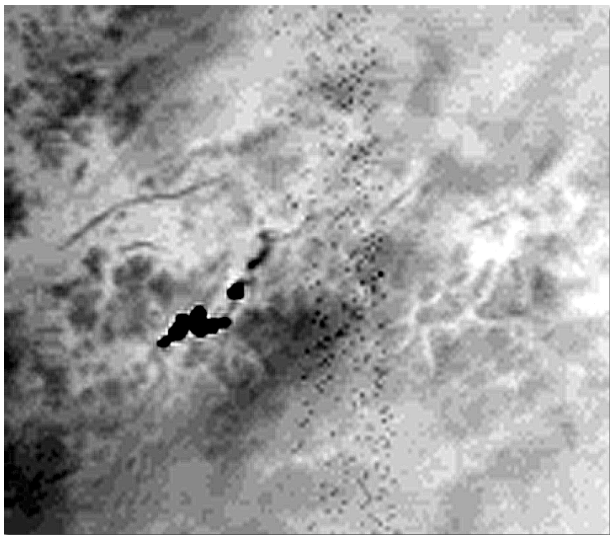

Figure 2. Visible light detection of the fireball dust cloud from space. This image was captured by the Defence Meteorological Satellite Program F-13 satellite. The satellite scanned through the dust trail (dark cloud left of center) approximately two minutes after the passage of the fireball. The image has been inverted for clarity.

2. CALCULATION OF THE FIREBALL TRAJECTORY, VELOCITY, INITIAL MASS AND ORBIT

2.1. Velocity and Atmospheric path

To compute the fireball trajectory we first make use of eyewitness data. In total over 90 persons were interviewed and measurements made of the observed path of the fireball in the Yukon and British Columbia. These data, however, are widely discordant and do not provide a good estimate for the complete trajectory. In particular, the slope of the fireball path in the atmosphere is particularly uncertain from these data. However, sufficient visual observations exist close to either side of the ground track to strictly constrain the fireball apparent radiant azimuth to be in the range $327^\circ \leq \phi \leq 334^\circ$. Using the best eyewitness data and the least-squares solution method of Borovicka (1990), the formal trajectory solution (with formal error) is given in Table 1. Note that this solution does not make use of the observers proximate to the ground track as these were observations of the dust cloud only. The relatively flat trajectory of the fireball is qualitatively reflected in numerous visual observers who (incorrectly) reported following the fireball to the southern horizon. The eyewitness solution should be treated very cautiously as the real errors are much larger than the formal error margins shown. Indeed, solutions with entry values from near zero to 25° and azimuths from 320° to nearly 350° may be accommodated with different (subjectively chosen) subsets of the eyewitness reports using the least-squares technique.

More accurate determination of the trajectory is possible by making use of the photographs and video of the associated dust cloud. In particular, three were made very shortly after the fireball, had good positional references in the fields of view, and were well separated spatially so as to provide a good intersection solution. An example of one of these is given in Figure 3. These observations consist of a video recordings made from Whitehorse (60.718°N; 135.054°W)(Wheeler) beginning 15 seconds after the fireball, a still photo of the dust cloud from 60.367°N; 134.089°W approximately 120 seconds after the event (Ford) and finally a still digital photo of the dust cloud from Atlin, British Columbia (59.572°N; 133.703°W) taken roughly 90 seconds after the fireball (Lemke).

To better resolve the original trajectory, the video record from Whitehorse was used to examine the upper wind motions. By following the dust cloud over a period of several minutes, the local wind vectors may be defined at different points along the trail. To determine the best fits for each observation, the same points on each trail were identified and the approximate wind vectors were inverted to reconstruct the original fireball trail – this iterative process was stopped when the modelled dust trails became nearest to linear at each site. Using the resulting appar-

Figure 3. Dust cloud photo taken from Atlin, British Columbia by Ewald Lemke.

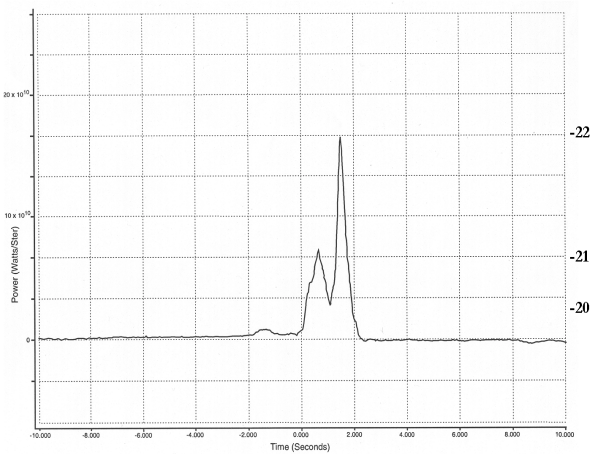

Figure 4. Optical satellite light curve. The right axis shows approximate absolute visual magnitude assuming a 6000K blackbody. Zero time is 16:43:42s UT on 18 January, 2000.

ent trajectories plus the original dust cloud measurements, a best-fit trajectory was determined as shown in Table 1.

To compute the velocity, common features in the optical light curve were compared with the infrared satellite measurements. From this comparison a mean velocity prior to the main burst of 15.5±0.6 kms^{-1} was found. Comparison of the satellite optical light curve and measured features on the most detailed dust cloud photos (Lemke) yield a velocity of 15.7 kms^{-1} prior to the main burst and velocities approaching 9 kms^{-1} at the end of the visible light curve.

Taking the satellite-determined fireball radiant altitude and azimuth as most accurate and an initial velocity of 15.8±0.6 kms^{-1} (corrected for early deceleration of the large pre-atmospheric meteoroid as shown in the next section) the orbit solution is shown in Table 2. The orbit is similar to previously measured meteorite orbits, having a Tisserand value of 3.6 and 1/a=0.5. However, these values would not rule out classification as an Encke-type cometary orbit.

2.2. Initial Mass

A measure of the initial mass of the meteoroid comes from satellite records of the event. Figure 4 is the lightcurve associated with the fireball recorded by US Department of Defence satellites. Assuming the bolide radiates as a 6000K blackbody, the integrated optical light energy from the fireball is 1.1×10^{12}J. The results of the St. Robert fireball/meteorite fall (Brown et al., 1996; Hildebrand et al., 1997) had both cosmogenic nuclide activities from recovered meteorites (which constrained the entry mass (Herzog et al., 1997)) and satellite data available to yield an apparent luminous efficiency (τ) of 10% in the silicon pass-band of the satellite sensor for this H-chondrite. Using this conversion efficiency as well as the integrated optical energy and the initial velocity determined from the previous section we derive an initial mass estimate near 9×10^4 kg. Given the unusual makeup of Tagish Lake as compared to H-chondrites, we anticipate this efficiency will be somewhat different. Taking a range of physically probable efficiencies to be from 5-20%, implies probable mass ranges from 5×10^4–1.8×10^5 kg.

To better estimate this initial mass, we use the entry model employed to interpret the lightcurve and initial mass for the St. Robert fireball (Brown et al., 1996), namely that of the gross fragmentation model of Ceplecha et al. (1993). Here we adopt the entry angle, initial velocity, apparent heights of initial break-up and satellite observed light curve as constraints for the modelling. Our goal is to determine the initial mass, using only a constant ablation coefficient as an assumed input. We note that the light so-produced is referenced to the revision in the panchromatic luminous efficiency scale computed by Ceplecha (1996) from analysis of the Lost City meteorite fall of 5.2%. We expect that for such a fragile body that the value for the ablation coefficient (σ) will be larger than chondritic values and most likely in the range 0.04 - 0.20 $sec^2 km^{-2}$. The implication of this larger σ is that the effective luminous efficiency will be higher than the ordinary stoney value (cf. ReVelle, 1983) and our estimates extreme upper limits (within the constraints of an assumed constant ablation coefficients). In particular, using a σ=0.02 s^2km^{-2} and a shape-density factor, K=0.46 (appropriate to type I fireballs) we compute an upper limit for the initial mass of 115 Tonnes.

To examine the effects of changing σ, particularly to (more realistic) higher values, we use the mean value for type II fireballs (which are believed to be associated with carbonaceous chondrites) as given in Ceplecha et al. (1998). Here we take σ=0.042 sec^2km^{-2} and K=0.69 to again fit the light curve. This produces a nominal mass estimate of 97 tonnes. Extending this to higher σ makes matching the light

curve and other observed parameters effectively impossible due to the simplification of using a constant ablation coefficient. However, recognizing the intrinsically higher τ values associated with such a porous object as noted by ReVelle (1983) and the higher effective σ associated with the extensive fragmentation, we regard both of the above estimates as upper limits to the true mass.

2.3. Seismic Data

In addition to satellite and ground-based photos/videos, the airwaves generated by the passage of the meteoroid were detected at several seismic stations. Other work has demonstrated the utility of deriving parameters for bolide trajectories from seismic data alone (cf. Qamar, 1995) when numerous stations detect the airwave. In the present case, however, only two seismic stations showed strong signals from the fireball and one other a weak probable signal. Fortunately, the entry geometry has been well-defined from satellite data.

The airwave from a meteoroid can be recorded as seismic waves in several ways. First, the airwave itself may force transverse oscillations at the Earth's surface due to the overpressure of the wavefront; these we call air-coupled Rayleigh waves. Secondly, the acoustic wave may match the natural seismic wave velocities in the ground and excite these modes directly; these we term air-coupled body waves, usually p-type seismic (longiutudal) waves.

The seismic station near Whitehorse (WHY) recorded a large impulsive (and relatively long lasting signal) beginning 208s after the main detonation recorded by the satellite (at 16:43:43 UT). Using a high-pass filter on these data (1 Hz and higher) we also note an emergent waveform beginning some 128s after the main detonation time. These phases are shown in Figure 5.

The strongest arrival is associated with the main airwave. We suggest this signal records the first direct arrival of the airwave from the ballistic shock, having started to propagate from the trajectory as a cylindrical blast wave. Rayleigh waves moving at near acoustic velocities in the topmost portion of the soil near the seismic station arrive next. The earliest arrival of the airwave phase is that of an N-wave signature in the vertical component of the seismograph (showing strong downward motion), indicative of that expected of shock loading of the local terrain (cf. Kanamori et al., 1991). The large amplitude of this arrival phase is typical of air-coupled Rayleigh waves which often are the strongest component of seismic records of airblasts due to resonant coupling with loose soil (Ewing et al. 1967).

The earlier P-wave (body wave) arrival is interpreted as resulting from sound coupling near the subterminal point of the fireball, where the sound first reaches the earth. Indeed, provided the amplitude of

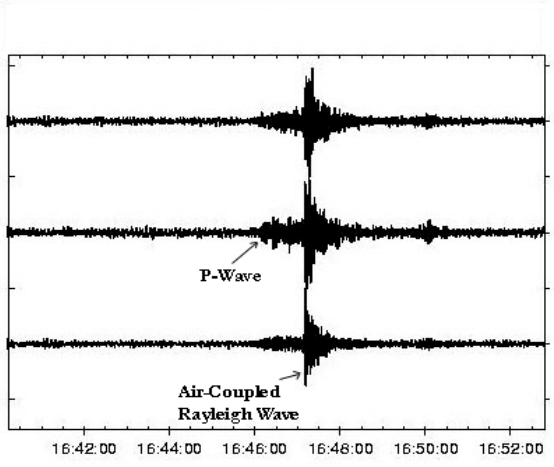

Figure 5. High-pass (1 Hz) filtered seismic record from WHY showing P-wave and Rayleigh wave arrivals. The three components shown are (from top) the E, N and Z-components. Amplitudes are normalized within each component.

the blast is sufficient, we expect the shock to couple directly into the ground very near the locus of points directly under the trajectory where the trace velocity across the ground of the cylindrical blast wave is comparable to the local P-wave velocity (which we adopt as 6 $\mathrm{km}s^{-1}$). Thus, the earliest P-wave signal should be from the region nearest the terminal portion of the fireball where a significant blast wave is still produced. Our final P-wave solution times and heights are relatively insensitive to values for upper crustal P-wave velocity different from the above. The effect of lower P-wave speeds (which would be the expected trend in a mountainous region) will be to push the solution to slightly higher heights.

To further examine the question of the origin of these seismic waves, we have taken the fireball trajectory determined from the satellite data as being most representative of the trajectory and modelled the expected arrival times of waves at WHY. We have used radiosonde data from WHY taken at 12 UT on Jan 18, 2000 as an input atmosphere to an altitude of 30 km and used the MSIS-E NASA atmosphere model above this height to define the acoustic velocity as a function of height. Ignoring wind corrections to this apparent sound velocity, we have computed the airwave arrivals at WHY as a function of height along the fireball path. Similarly, we compute the arrival times for P-waves, using the previously described model of the airblast travelling to ground then the P-waves travelling to the seismic station. A graphical version of the resulting solution is shown in figure 6.

A priori, ignoring fragmentation (which produces quasi-spherical symmetry along the trajectory) we expect the ballistic-weak-shock to propagate approximately normal to the fireball trajectory (cf. Revelle, 1976). As a result, this airwave should have an origin from that portion of the trajectory of the fireball passing closest to the station. In figure 6 this would

be the minimum in the parabolic time propagation curve. In fact, the large-amplitude acoustic arrival occurs almost 20 seconds after this point.

To determine if this discrepancy is due to our ignoring the upper winds in calculation of the sound velocity, we have numerically modelled ray arrivals to the station from along the fireball trajectory. This simulation uses the same atmosphere as described earlier, but explicitly takes into account the wind velocity and ray propagation geometry in computing ray arrival times. As the wind velocity was very high near 30km altitude (almost 70 m/s), we expect this may produce significant deviations from our nominal curves, making the sound velocity a function of propagation azimuth.

The model results for propagation from various source heights are shown in figure 6 as solid squares. The wind effects are clearly evident and account nicely for the timing difference. Where several rays reach WHY we have shown the extreme range in arrival times for a given height. The numerical results suggest that the beginning of the main seismic signal (and the largest amplitude) is indeed from the ballistic wave propagating nearly normal to the fireball path, with significant modifications from the upper wind.

The main seismic signal beginning 208s after the detonation continues for approximately 84s. This is longer than would be expected if only the portion of the trail near the specular point were contributing the airwave signal where dispersion effects which spread the acoustic signal in time are minimal. Anglin and Haddon, 1987 and Cumming, 1989 both show examples of air-coupled seismic waves from bright fireballs - in both cases the signals persist for $\leq$10 seconds. In our records, there are several additional maxima during this 84 second window. While some contribution from the P-wave may be present early in the record, it is unlikely to persist for this entire interval or show such localized maxima. We note that the extended signal could be a consequence of the properties of the soil proximal to the seismograph or the result of sound reflecting off the steep local terrain. No simple means of determining if extended resonance effects are significant due to local ground properties or sound reflection; we can only indicate that these are not seen for fireball airwaves recorded by other seismic instruments at different locations.

One interpretation of this extended signal is that it represents acoustic energy from ongoing gross fragmentation not represented in the cylindrical blast wave model and propagating in a wider suite of directions (ReVelle, 1976) to WHY. Such a model would suggest arrivals at WHY from the terminal portions of the fireball where the satellite light curve shows significant ablation and (by inference) possibly fragmentation. This is similar to the interpretations of Cumming (1989) and Folinsbee et al. (1969) where seismic data were compared to photographically determined fireball trajectories and suggested almost all the acoustic signal was due to energy generated near the terminal portions of the trajectory. In both cases these locations were significantly different than the closest points along the trajectory relative to the receiving seismic stations.

Examining figure 6 we see that the numerical ray modelling shows acoustically accessible paths from heights along the trajectory restricted to those greater than 37 km altitude. Our numerical modelling reveals that lower heights may produce acoustical signatures, but these are just inside the first acoustic shadow zone of the sound as seen from WHY and would not contribute significantly to the seismic signal. Figure 8 demonstrates this effect.

That the numerical arrival times end within 10 seconds of the cessation of the main seismic signal suggests that fragmentation along the latter portion of the path is a plausible production mechanism for the extended signal. We also note that while heights along the fireball path below 38 km will not contribute significantly to the signal, our ray modelling is a geometrical approximation which ignores scattering and diffraction effects whereby lower portions of the trajectory may contribute to some of the trailing end of the main signal.

On the basis of seismic data from WHY, we suggest that the major portion of the large scale fragmentation for the Tagish Lake fireball ended near 32 km altitude. The seismic solution for station HYT is shown in figure 7 and supports this height determination. The WHY seismic record also suggests that this fragmentation dominated the last 45–60 km (3-4 seconds of travel through the atmosphere) of the path in agreement with the satellite light curve which shows almost 4 seconds of noticeable signal (corresponding to $\approx$60 km along the path at the nominal initial entry velocity).

3. PHYSICAL INTERPRETATION

3.1. Meteorites

The meteorites recovered from the Tagish Lake fireball have been classified as C2, ungrouped. They represent a primitive form of carbonaceous chondrite, perhaps the most primitive meteorite studied to date (cf. Brown et al., 2000). Recent studies of the reflectance spectra from powdered Tagish Lake material also suggest a linkage with D-class asteroids (Hiroi et al., 2001). This represents the first connection between D-class asteroids and meteoritic material. This also supports the supposition that Tagish Lake material is primitive, given the presumed supercarbonaceous origins for the D-class asteroids (cf. Bell et al., 1989).

To further examine the physical character of the original Tagish Lake object, we have measured the densities and porosities of two Tagish Lake specimens.

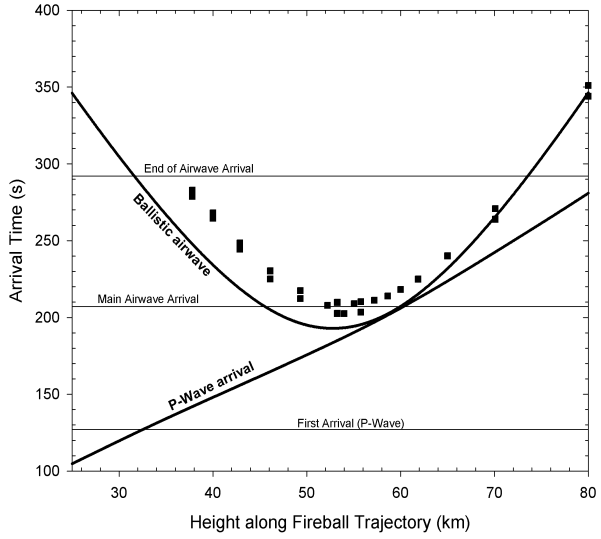

Figure 6. Seismic wave arrival times (labelled horizontal lines) and nominal air wave arrival times at WHY using a mean sound velocity as a function of height along the fireball trajectory (parabolic line). The zero time is the time of the fireball main detonation (16:43:43 UT). Also shown is the solution for P-wave arrivals. Square symbols represent numerical solutions from ray-path modelling (including wind effects) at each height to WHY as described in the text. These model solutions show those heights at which acoustic ray paths to WHY exist - this does not imply actual acoustic signals arrive from such heights as this also depends on the source generation mechanism, i.e. ballistic cylindrical shock vs. fragmentation. All modelled travel times have been corrected for the fireball's velocity.

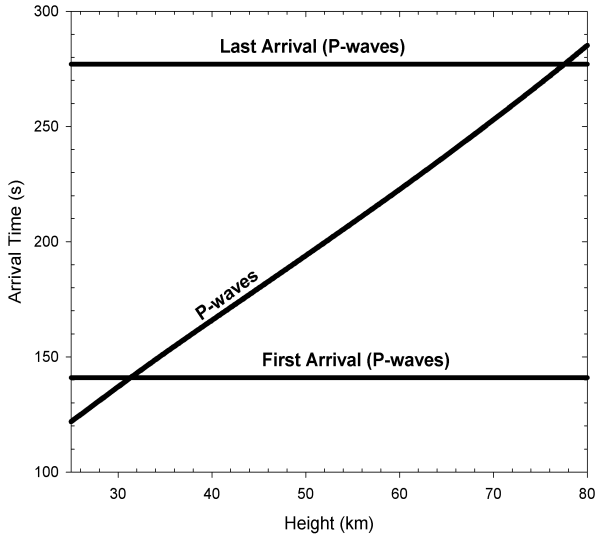

Figure 7. Seismic wave arrival times (labelled horizontal lines) at HYT using a mean sound velocity as a function of height along the fireball trajectory. The zero time is the time of the fireball main detonation (16:43:43 UT). Also shown is the solution for P-wave arrivals. All modelled travel times have been corrected for the fireball's velocity.

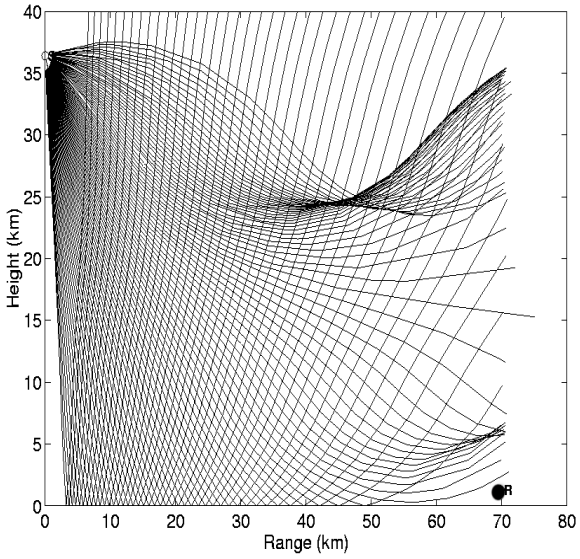

Figure 8. Acoustic ray paths from the location of the main burst to WHY (labelled as R in the lower right-hand corner of the figure). Notice the lack of rays reaching the receiver for this combination of height and range.

The results are shown in Table 2. The porosity and bulk density for Tagish lake are among the lowest yet measured for meteorites. Only the Orgueil CI-chondrite has been reported with comparable porosity and bulk density, though controversy exists as to whether these low values may be due to weathering effects (cf. Corrigan et al., 1997).

We expect that the material recovered from Tagish Lake preferentially represents the strongest portions of the original brecciated body. The implication of these measurements is that the original pre–atmospheric Tagish lake meteoroid had comparable or higher porosities and lower bulk densities to those given in Table 2. This would imply probable porosities of order $\geq$40%.

3.2. The Fireball

To attempt to place the Tagish Lake fireball in the context of physical data available for other fireballs, we make use of the PE-criterion introduced by Ceplecha and McCrosky (1976). This statistical index is a proxy measure for the relative physical strength of the associated meteoroid based on the ability of the associated fireball to penetrate the atmosphere. More specifically, the PE-criterion is given by

$$PE = \log(\rho_E) - 0.42\log(m_\infty) + 1.49\log(V_\infty)$$

$$-1.29\log(cos(Z_R))$$

where ρ_E is the air density at the fireball end-point, m_∞ is the initial mass, V_∞ is the initial velocity and Z_R is the zenith angle of the trajectory. Ceplecha and McCrosky (1976) suggested four basic physical groupings existed in the fireball record, from the strongest, most penetrating material (Group I) to the weakest material (Group IIIb). These groupings have been associated with (cf. Ceplecha et al., 1998), ordinary chondrites, carbonaceous chondrites, strong cometary material and weak cometary material for groups I, II, IIIa and IIIb respectively. We emphasize that the exact PE values where one group ends and another begins is somewhat uncertain as this is a purely statistical measure. From our best estimate for the initial mass of the Tagish Lake object (65 tonnes), its initial velocity (15.8 km/s), its known zenith angle at entry (72.2°) and the last observed dust cloud "point" from the ground based data of 29 km, we arrive at a PE=-5.39. This is near the border of the Type II and IIIa groups (which split at PE=-5.25). Given the statistical uncertainties in the broader groups, we suggest that Tagish Lake represents the low end of the strength spectrum for carbonaceous chondrites or the very highest end of the cometary strength spectrum. This is consistent with the physical evidence from the meteorites.

4. DISCUSSION AND CONCLUSIONS

From the above evidence, we suggest that Tagish Lake represents an object which physically bridges the population of cometary objects and the weakest "asteroidal" material existing in meteorite collections. The high porosity of measured fragments as well as the higher inferred porosity of the initial object all suggest a weakly structured object. That any material reached the surface for collection is almost certainly the result of the large initial mass, low entry angle (and hence lower dynamic pressures) coupled with the region of the fall. We speculate that Tagish Lake–type material landing in warmer and wetter climates would be quickly eroded into chips and dust.

Of particular interest is the spectral connection between Tagish Lake and D-class asteroids (cf. Hiroi et al., 2001). We note that the only probable D-class asteroids to have accurate density determinations are Phobos and Deimos (cf. Britt and Consolmagno, 2000). Currently, the most accurate bulk densities for Phobos are 1.53±0.1 gcm^{-3} and 1.34±0.83 gcm^{-3} for Deimos (Smith et al., 1995). Comparison with Tagish Lake shows that the bulk densities are (within error) the same as the bulk density measurements for Tagish Lake. The high porosity of Tagish Lake samples (≈40%) indicates that both Martian moons need not have significant macroporosity and suggests that appeals to large amounts of interior ice or a thick regolith (eg. Smith et al., 1995) to account for the low bulk density of the Martian moons may be unnecessary.

REFERENCES

Anglin, F. M. & Haddon, R. A. W. 1987, Nature, 328, 607

Bell, J. F., Davis, D. R., Hartmann, W. K., & Gaffey, M. J. 1989, Asteroids II, 921

Borovicka, J. 1990, Bulletin of the Astronomical Institutes of Czechoslovakia, 41, 391

Britt, D. T. & Consolmagno G. J., 2000, Icarus, 146, 213

Brown, P. G. et al. 2000, Science, 290, 320

Brown, P. et al. 1996, Meteoritics and Planetary Science, 31, 502

Ceplecha, Z. & McCrosky, R. E. 1976, Journal of Geophysical Research, 81, 6257

Ceplecha, Z. 1996, Astronomy & Astrophysics, 311, 329

Ceplecha, Z., Spurny, P., Borovicka, J., & Keclikova, J. 1993, Space Science Reviews, 279, 615

Ceplecha, Z. ;. K., Borovička, J. ;. Í., Elford, W. G., Revelle, D. O., Hawkes, R. L., Porubčan, V. ;., & Šimek, M. ; 1998, Space Science Reviews, 84, 327

Corrigan, C. M., Zolensky, M. E., Dahl, J., Long, M., Weir, J., Sapp, C., & Burkett, P. J. 1997, Meteoritics and Planetary Science, 32, 509

Cumming, G.L., 1989, Canadian Journal of Earth Science, 26, 1350

Ewing, W.M., Jardetsky, W.S., & Press, F., Elastic Waves in Layered Media, McGraw-Hill, New York, 1967

Herzog, G. F. et al. 1997, Meteoritics & Planetary Science, vol. 32, page A59, 32, 59

Hildebrand, A. R. et al. 1997, JRASC, 91, 261

Hiroi, T., Zolensky, M. E., & Pieters, C. M. 2001, Lunar and Planetary Science Conference, 32, 1776

Kanamori, H., Anderson, D. L., Mori, J., & Heaton, T. H. 1991, Nature, 349, 781

Keay, C. S. L. 1980, Science, 210, 11

Qamar, A. 1995, Seismological Research Letters, 66, 6

ReVelle, D.O. 1983, Meteoritics, 18, 386

Revelle, D. O. 1976, Journal of Geophysics Research, 81, 1217

Smith, D. E., Lemoine, F. G., & Zuber, M. T. 1995, Geophysical Research Letters, 22, 2171

Table 1. Trajectory solutions for the Tagish lake fireball using eyewitness data, the best three ground-instrumental records and satellite records. Shown are the apparent azimuth(ϕ) and altitude(θ) of the apparent radiant; the longitude (λ) and latitude (δ) of the main burst, and the estimated height of the main burst

Solution	ϕ	θ	Main Burst (λ,δ)	Height of main burst (km)
Eyewitness	319±2.6°	9.1±3.0°	134.630±0.18°,59.99±0.11°	31.4±2.7
Video&Photographic	330.7°±2.4°	14.5°±1.6°	134.645°,60.040°	37.6±1.7
Satellite	330.7°	17.8°	134.6°,60.02°	35

Table 2. Orbit for the Tagish Lake fireball using the satellite recorded trajectory solution. All angular coordinates are J2000.0

V_∞	15.8±0.6 kms^{-1}
α_G	89.9±2.2°
δ_G	29.8±2.4°
a	2.0±0.2 A.U.
e	0.56±0.04
q	0.885±0.010 A.U.
ω	223.9±2.2°
Ω	297.901±0.001°
i	2.0±0.9°
Q	3.2±0.4 A.U.

Table 3. Densities and porosities of two Tagish Lake meteorites. M(g) is the measured mass in grams while mineral ρ is the grain density of the specimen (gcm^{-3}) as measured by a helium pycnometer. The bulk ρ is the bulk density computed from the mass and volume (measured using glass beads). The porosity is a measure of the void space in the object and is computed from the grain density and mass. Data for Orgueil (CI chondrite) and other meteorite class averages are taken from Britt and Consolmagno (2000).

Sample	M(g)	Mineral ρ	Bulk ρ	Porosity (%)
Tagish Lake (RB)	30.44	2.74	1.65±0.15	40±10
Tagish Lake (ET-06)	77.19	2.56	1.61±0.10	37±6
Orgueil	47.2	2.43	1.58±0.03	35±7
H-Chon (Av.)	-	3.70	3.46	5
CM-Chon (Av.)	-	2.71	2.21	12